Journal of Materials Chemistry A



PAPER

View Article Online
View Journal | View Issue



Cite this: J. Mater. Chem. A, 2020, 8, 13735

Received 17th March 2020 Accepted 24th June 2020

DOI: 10.1039/d0ta03058a

rsc.li/materials-a

Effects of linking units on fused-ring electron acceptor dimers†

Guilong Cai,^{ab} Yiqun Xiao,^c Mengyang Li,^d Jeromy James Rech, ^{be} Jiayu Wang,^b Kuan Liu,^b Xinhui Lu, ^{bc} Zheng Tang,^d Jiarong Lian,^{*a} Pengju Zeng,^a Yiping Wang,^a Wei You ^{be} and Xiaowei Zhan ^{b*b}

Three fused-ring electron acceptors (SIDIC, DIDIC and TIDIC) were designed and synthesized using single bond, vinylene and acetylene units linked indaceno[3,2-b]dithiophene dimers as electron-rich cores and 3-(1,1-dicyanomethylene)-5,6-difluoro-1-indanone as electron-deficient termini. These molecules exhibit strong absorption from 550 to 900 nm with large attenuation coefficients of $1.8-2.0 \times 10^5 \, \text{M}^{-1} \, \text{cm}^{-1}$ and high electron mobilities of $2.2-4.9 \times 10^{-3} \, \text{cm}^2 \, \text{V}^{-1} \, \text{s}^{-1}$. In combination with wide-bandgap polymer FTAZ as a donor, organic solar cells exhibit efficiencies of 9.3-13.1%. Effects of the linking units on optical, electronic, morphologic, and photovoltaic properties were revealed. Relative to SIDIC, vinylene-bridged DIDIC shows red-shifted absorption, while acetylene-bridged TIDIC shows blue-shifted absorption. Compared with SIDIC and DIDIC, TIDIC has a lower HOMO, higher electron mobility, and higher device efficiency.

Introduction

Organic solar cells (OSCs) with bulk heterojunction (BHJ) structure have received increasing interest as a potential green energy conversion technology since they have unique strengths, for example, easy processing, light weight, low cost, flexibility and semi-transparency. The BHJ photoactive layers consist of electron donors (D) and acceptors (A). While fullerenes were the dominant acceptors during last 20 years, the drawbacks of poor visible light absorption, restricted energy level adjustability, and morphology instability, have spurred the design of new types of acceptors. To address these issues, various nonfullerene acceptors have been developed since they have intense light absorption in visible and near-infrared (NIR) regions and tunable energy levels. The series of the series of

The acceptor-donor-acceptor based fused-ring electron acceptors (FREAs) represented by ITIC8 and IDIC9 were first pioneered by the Zhan group. FREAs are typically comprised of an electron-rich fused-ring core like indaceno[3,2-b]dithiophene (IDT) and two electron-deficient termini like 1,1dicyanomethylene-3-indanone. FREAs exhibit high electron mobility (μ_e), strong visible-NIR absorption and high exciton diffusion coefficient,10 and their OSCs exhibit high power conversion efficiency (PCE), low energy loss and good stability.5 Now, most developments in this field focus on molecular engineering to modify the central cores, 11-17 side substituents18,19 and termini,20-25 leading to continually breaking efficiency records.26-32 All the high-performance FREAs are based on fused-ring cores, and their optoelectronic properties are generally modulated via tailoring the fused-ring cores, such as extending the core size,17 isomerization33 and asymmetric structure.34 However, all these approaches generally use relatively complex and lengthy synthesis routes, leading to overall low yields and high cost. Using simple and cheap donor/ acceptor/bridging units to synthesize electron acceptors in high yields is relatively easy to scale up and can reduce cost. 35-38

Several organic semiconductors based on single bond, vinylene and acetylene linking units have been used for phototransistors and field-effect transistors, *etc.* ³⁹⁻⁴¹ Compared with single bond- and vinylene-linked materials, the acetylene-linked materials generally show blue-shifted absorption spectra due to the electron-deficient nature of the acetylene unit. Nevertheless, there have been no any works to compare effects of single bond, vinylene and acetylene linking units in nonfullerene acceptors on photovoltaic properties.

^aKey Laboratory of Optoelectronic Devices and Systems of Ministry of Education and Guangdong Province, College of Physics and Optoelectronic Engineering, Shenzhen University, Shenzhen 518060, China. E-mail: ljr@szu.edu.cn

^bDepartment of Materials Science and Engineering, College of Engineering, Key Laboratory of Polymer Chemistry and Physics of Ministry of Education, Peking University, Beijing 100871, China. E-mail: xwzhan@pku.edu.cn

Department of Physics, The Chinese University of Hong Kong, New Territories 999077, Hong Kong, China

^aCenter for Advanced Low-dimension Materials, State Key Laboratory for Modification of Chemical Fibers and Polymer Materials, College of Materials Science and Engineering, Donghua University, Shanghai 201620, China

^eDepartment of Chemistry, University of North Carolina at Chapel Hill, Chapel Hill, North Carolina 27599, USA

[†] Electronic supplementary information (ESI) available. See DOI: 10.1039/d0ta03058a

Fig. 1 Chemical structures of SIDIC, DIDIC, TIDIC and FTAZ.

In this study, we designed and synthesized 3 new FREAs based on IDT dimer cores: SIDIC, DIDIC and TIDIC (Fig. 1). The optoelectronic properties can be tuned by changing the simple bridges (single bond, vinylene and acetylene) between two IDT units. Particularly, the vinylene and acetylene units were firstly introduced into the FREAs as linking units. The cells based on wide-bandgap polymer FTAZ as a donor and TIDIC as an acceptor display a best PCE of 13.1%, notably exceeding those of SIDIC and DIDIC-based cells (11.0 and 9.3%, respectively). This synthetic approach uses commonly-used IDT and simple bridging units to construct high-performance dimers, and therefore is easier to scale up than complex core extension and isomerization routes.

Results and discussion

Synthesis and characterization

Scheme S1 in ESI† presents synthetic routes of **SIDIC**, **DIDIC** and **TIDIC**. The chemical structures of new compounds were characterized by elemental analysis, ¹H and ¹³C NMR, and MS (see ESI†). **SIDIC**, **DIDIC** and **TIDIC** have good solubility in routine organic solvents like chloroform. In accordance with thermogravimetric analysis (TGA) (Fig. S1†), **SIDIC**, **DIDIC** and **TIDIC** are thermally stable up to >300 °C (Table 1).

All compounds in solution have intense absorbance from 550-850 nm with large molar attenuation coefficients of $1.8-2.0 \times 10^5 \text{ M}^{-1} \text{ cm}^{-1}$ (Fig. S2†). The absorption peaks of **TIDIC**, **SIDIC** and **DIDIC** red shift gradually, and all thin film absorption spectra also red shifts by 26-52 nm compared with those in

solution (Fig. 2a). The optical bandgaps (E_g) of **SIDIC**, **DIDIC** and **TIDIC**, evaluated from the absorption edges of their thin films, are 1.43, 1.40 and 1.55 eV, respectively (Table 1).

Next, cyclic voltammetry (CV) was performed to understand the impact of the bridging units on the electronic properties. The CV of **SIDIC**, **DIDIC** and **TIDIC** (Fig. S3†) was used to estimate the lowest unoccupied molecular orbital (LUMO) and highest occupied molecular orbital (HOMO) energies using corresponding inflection points for reduction and oxidation potentials in reference to the half-wave potential for FeCp₂^{+/} redox couple. The LUMO energies of **SIDIC**, **DIDIC** and **TIDIC** are -3.88, -3.91 and -3.88 eV, while the HOMO energies are -5.43, -5.44 and -5.59 eV, respectively (Fig. 2b). Three molecules have similar LUMO, while **TIDIC** has a down-shifted HOMO relative to **SIDIC** and **DIDIC**, due to electron-deficient acetylene bridge.

Another important characteristic to understand is impact of the different bridging units on charge transport properties. The μ_e of **SIDIC**, **DIDIC** and **TIDIC** are 3.4×10^{-3} , 2.2×10^{-3} and 4.9×10^{-3} cm 2 V $^{-1}$ s $^{-1}$, respectively (Table S3†), in accordance to space charge limited current (SCLC) measurement (Fig. S4†). These values are similar to those of fullerene acceptors ($\sim\!10^{-3}$ cm 2 V $^{-1}$ s $^{-1}$), 43 ensuring to effectively transport electrons from the active layer to the cathode.

Photovoltaic properties

The wide-bandgap polymer **FTAZ** (Fig. 1) was chosen as a donor to fabricate OSCs since its intense absorption at 400–650 nm ⁴⁴

Table 1 Basic properties of SIDIC, DIDIC and TIDIC

		λ_{\max}^{b} (nm)					
Compound	$T_{\mathbf{d}}^{a}$ (°C)	Solution	Film	$\varepsilon^{c} \left(M^{-1} \text{ cm}^{-1} \right)$	E_{g}^{d} (eV)	$HOMO^{e}$ (eV)	LUMO ^e (eV)
SIDIC	329	728	759	$2.0 imes 10^5$	1.43	-5.43	-3.88
DIDIC TIDIC	305 349	737 675	789 701	$1.9 imes 10^{5} \ 1.8 imes 10^{5}$	1.40 1.55	-5.44 -5.59	-3.91 -3.88

 $[^]a$ Decomposition temperature measured by TGA. b Absorption maximum. c Molar attenuation coefficient at λ_{\max} in solution. d Optical bandgap calculated from the absorption edge of thin film. e Estimated from the onset oxidation/reduction potentials in cyclic voltammograms.

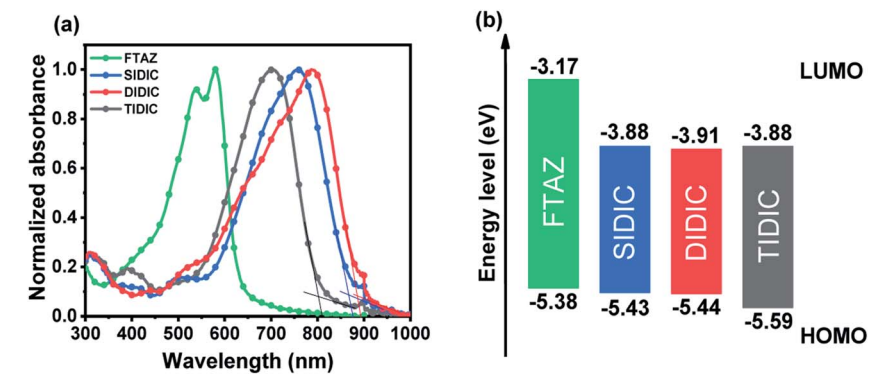


Fig. 2 (a) UV-vis absorption spectra of FTAZ, SIDIC, DIDIC and TIDIC in thin films. (b) Energy levels of FTAZ, SIDIC, DIDIC and TIDIC estimated from cyclic voltammetry.

complements those of SIDIC, DIDIC and TIDIC (Fig. 2a) and its energy levels fit those of the acceptors (Fig. 2b).45 The OSCs have an inverted architecture of indium tin oxide (ITO) glass/ZnO/ FTAZ:acceptor/MoO_x/Ag. After optimization of donor/acceptor ratio (Table S1†) and the content of additive 1,8-diiodooctane (DIO) (Table S2†), the best cell based on FTAZ/TIDIC exhibits a PCE of 13.1% with a $V_{\rm OC}$ of 0.879 V, $J_{\rm SC}$ of 20.2 mA cm⁻², and FF of 73.6% (Fig. 3a and Table 2). The SIDIC-based devices show decreased performance with a $V_{\rm OC}$ of 0.863 V, $J_{\rm SC}$ of 18.4 mA cm⁻², FF of 69.4% and PCE of 11.0%. The **DIDIC**-based devices show the worst performance with a $V_{\rm OC}$ of 0.816 V, $J_{\rm SC}$ of 17.5 mA cm $^{-2}$, FF of 65.1% and PCE of 9.3%. The $V_{\rm OC}$ of OSCs based on DIDIC, SIDIC and TIDIC is gradually improved, which is consistent with the LUMO trend found from CV.

The external quantum efficiency (EQE) spectra of the optimized cells based on TIDIC, SIDIC and DIDIC gradually red shift (Fig. 3b), similar to the absorption trend of the acceptors. The maximum EQE of DIDIC, SIDIC, and TIDIC-based devices gradually increase from 66.1% to 73.8% and 80.7%, implying enhanced charge generation, leading to enhanced J_{SC} .

We measured photocurrent density (J_{ph}) versus effective voltage ($V_{\rm eff}$) of the cells (Fig. 3c) and used the $J_{\rm SC}/J_{\rm sat}$ ($J_{\rm sat}$: saturation photocurrent density) to characterize the charge collection under short-circuit condition. The $J_{\rm SC}/J_{\rm sat}$ ratio for the best devices based on SIDIC, DIDIC and TIDIC are 94.5%, 91.4% and 99.2%, respectively. The TIDIC-based device has superior charge collection efficiency than the SIDIC- and DIDICbased devices, which can also be used to describe the higher efficiency of FTAZ/TIDIC devices.

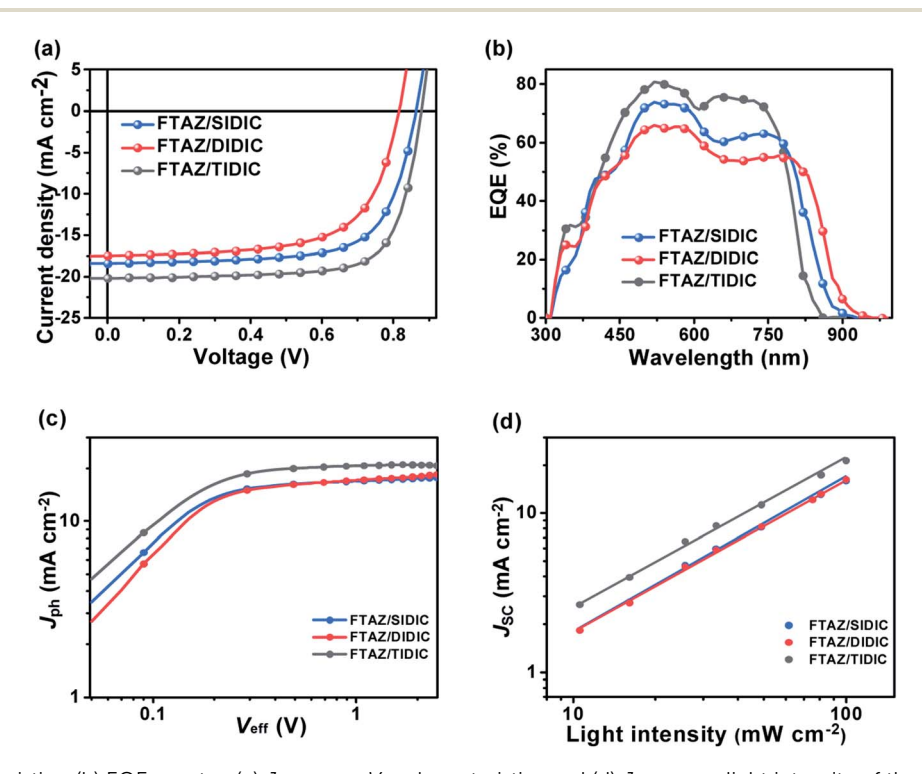
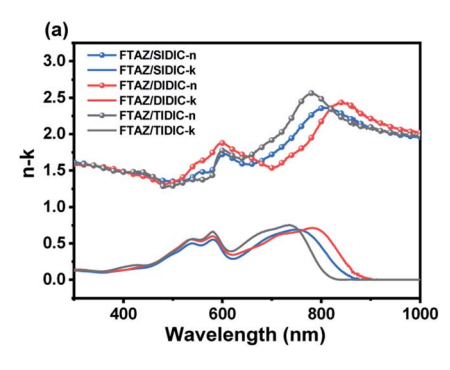


Fig. 3 (a) J-V characteristics, (b) EQE spectra, (c) J_{ph} versus V_{eff} characteristics and (d) J_{SC} versus light intensity of the optimized devices.

Table 2 Performance of the optimized OSCs based on FTAZ/acceptor

Device ^a	$V_{\mathrm{OC}}^{b}(V)$	$J_{\mathrm{SC}}^{}b}$ (mA cm $^{-2}$)	$\mathrm{FF}^{b}\left(\% ight)$	PCE^{b} (%)	Calculated $J_{\rm SC}$ (mA cm ⁻²)
SIDIC DIDIC TIDIC	$0.863 \ (0.858 \pm 0.005) \ 0.816 \ (0.817 \pm 0.001) \ 0.879 \ (0.869 \pm 0.006)$	$18.4~(17.9\pm0.3)$ $17.5~(17.1\pm0.3)$ $20.2~(20.6\pm0.4)$	$69.4~(68.4\pm1.4) \ 65.1~(64.0\pm1.0) \ 73.6~(70.7\pm1.4)$	$11.0~(10.5\pm0.3) \ 9.3~(8.9\pm0.3) \ 13.1~(12.7\pm0.2)$	18.3 17.7 19.6

^a FTAZ/acceptor = 1/1.5 (w/w), 0.2% DIO (v/v). ^b Average values (in parenthesis) are obtained from 20 devices.



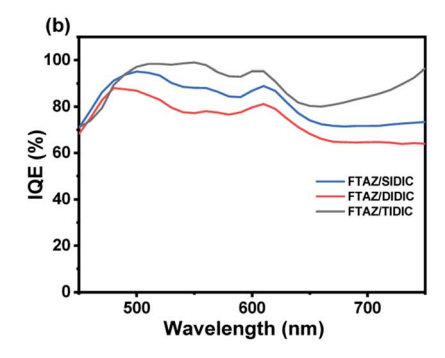


Fig. 4 (a) Optical constants (n, k) and (b) IQE of FTAZ/SIDIC, FTAZ/SIDIC and FTAZ/TIDIC.

Furthermore, the charge recombination dynamics was also probed by measuring each solar cell under varying intensity of incident light. The $J_{\rm SC}$ versus light density ($P_{\rm light}$) relationship can be expressed by $J_{\rm SC} \propto P_{\rm light}^{\alpha}$.⁴⁷ The slope of the curve (i.e. α value) provides insight to the strength of bimolecular recombination under the short-circuit condition. The α values of the SIDIC, DIDIC and TIDIC-based cells are 0.993, 0.995 and 0.986 (Fig. 3d), respectively, implying ignorable bimolecular recombination losses for all of solar cells under short-circuit condition.

While we presented the electron mobility of each acceptor alone earlier, the charge carrier mobilities in the BHJ blend are also very important. In accordance with the SCLC measurements⁴⁸ (Fig. S5†), the TIDIC-based blend exhibits high hole mobility (μ_h) of 2.5×10^{-3} cm² V⁻¹ s⁻¹ and μ_e of 1.1×10^{-3} cm² V⁻¹ s⁻¹ with a μ_h/μ_e ratio of 2.3 (Table S3†). The SIDIC and DIDIC-based blends display lower μ_h (0.75 × 10⁻³ and 1.2 × 10^{-3} cm² V⁻¹ s⁻¹) and μ_e (0.29 × 10^{-3} and 0.14×10^{-3} cm² V⁻¹ s⁻¹) with higher μ_h/μ_e ratio (2.6 and 8.6). Thus, the TIDIC-based blend films have higher and more balanced charge mobilities, which can minimize charge accumulation, contributing to a higher FF.

Interestingly, the **TIDIC**-based device has the highest J_{SC} , while the **DIDIC**-based device has the lowest J_{SC} , which is contrary to the absorption spectra where the absorption peak of **DIDIC** red shifts 88 nm compared to that of **TIDIC**. We measured the optical constants of the materials used in the solar cell stack (Fig. 4a), and found that attenuation coefficients of all the blends are very similar. However, the BHJ based on **FTAZ/TIDIC** has a narrower absorption spectrum compared to those of **FTAZ/DIDIC** and **FTAZ/SIDIC**. Therefore, the different J_{SC} is most likely due to different internal quantum efficiency (IQE) of the solar cells. IQE was calculated using the measured

EQE divided by the absorbance of the active layer, obtained by optical transfer matrix simulations. The simulations were performed using the measured optical constants of the materials. Indeed, IQE of the **TIDIC**-based device is the highest, while that for **DIDIC** is the lowest (Fig. 4b).

Film morphology

Having investigated the impact that the various bridging groups have on the electronic, optical, and photovoltaic properties of the resulting FREAs, we next searched for key morphological differences. The first preliminary investigation into the morphology was done with atomic force microscopy (AFM). This approach can provide surface images of the pure and blend films. The pure films of SIDIC, DIDIC and TIDIC show rootmean-square (RMS) roughness of 1.90, 2.68 and 0.77 nm, respectively (Fig. S6†). DIDIC has a rougher surface compared to SIDIC and TIDIC, which affects interfacial contact and electron transport, leading to lower mobility. All the optimized blends have similarly smooth surface with RMS roughness of 0.68, 0.92 and 0.90 nm, respectively (Fig. S7†). This leads us to explore morphology with more in-depth tools.

While AFM probes the surface, a deeper probe into the molecular packing is needed. Fig. 5 and S8† show the two-dimensional (2D) grazing incidence wide angle X-ray scattering (GIWAXS)⁴⁹ patterns and the intensity profiles of the blend and pure films. The **FTAZ/SIDIC** film exhibits predominant face-on orientation with the lamellar peak at $q_r = 0.32 \text{ Å}^{-1}$ (d = 29.6 Å) and the π - π peak at $q_z = 1.71 \text{ Å}^{-1}$ (d = 3.67 Å), which are attributed to the scattering of the crystalline **FTAZ** domains based on the consistent lattice constants. **SIDIC** shows low crystallinity in the blend film with no noticeable scattering peaks observed. The **FTAZ/DIDIC** film exhibits strong scattering peaks in the in-plane direction at $q_r = 0.27, 0.32, 0.39$ and 0.45

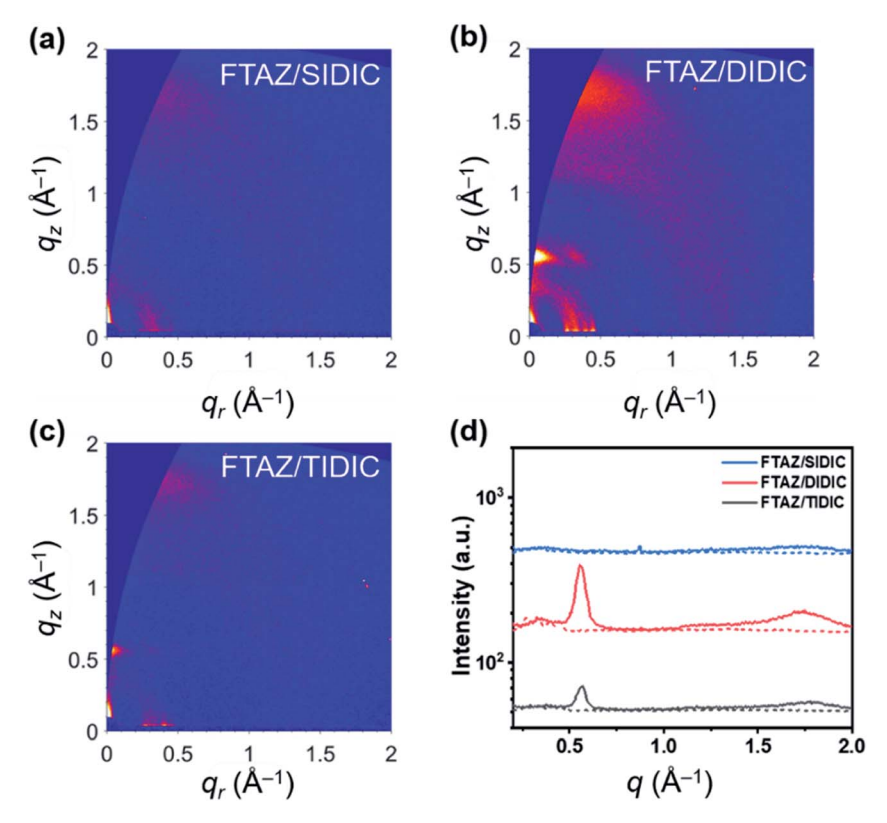


Fig. 5 GIWAXS patterns of (a) FTAZ/SIDIC, (b) FTAZ/DIDIC and (c) FTAZ/TIDIC blend films, and (d) the corresponding intensity profiles along the in-plane (dashed line) and out-of-plane (solid line) directions.

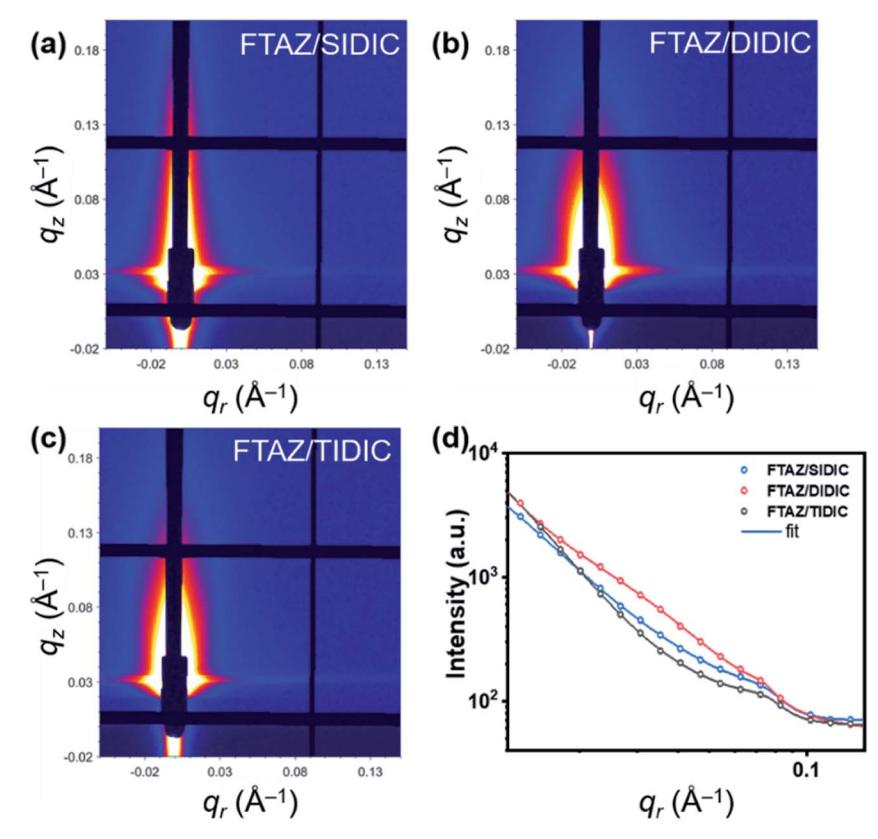


Fig. 6 (a-c) 2D GISAXS patterns of the blends. (d) The corresponding GISAXS profiles and best fittings along the in-plane direction.

 $\mathring{\mathbf{A}}^{-1}$, indicating preferential face-on packing. The peak at $q_{\rm r}=0.32~\mathring{\mathbf{A}}^{-1}$ can still be assigned to FTAZ, while the rest should come from the highly crystallized DIDIC domains. The FTAZ/TIDIC blend film also shows preferential face-on packing with the lamellar peak appeared at $q_{\rm r}=0.31~\mathring{\mathbf{A}}^{-1}$ ($d=20.3~\mathring{\mathbf{A}}$) and the π - π peak at $q_z=1.76~\mathring{\mathbf{A}}^{-1}$ ($d=3.57~\mathring{\mathbf{A}}$). There is another scattering peak at $q_{\rm r}=0.41~\mathring{\mathbf{A}}^{-1}$, which is possibly due to the end group π - π stacking of TIDIC along the backbone. In summary, the GIWAXS results demonstrate that all three acceptor blends can adopt a preferential face-on orientation and have π - π stacking which is appropriate for charge transport.

The molecular geometries of SIDIC, DIDIC and TIDIC were investigated with density functional theory (DFT) calculations B3LYP/6-31G* level (Fig. S9†). All three acceptor molecules possess highly planar backbones. In order to gain more insights into the effects of the linking units on the packing properties of the acceptors, we conducted potential energy surface scan with the dihedral angles between the two IDT planes (Fig. S10†). The value of rotation energy barrier of DIDIC is 394 meV, much higher than those of SIDIC (196 meV) and TIDIC (55 meV), suggesting DIDIC has the most rigid configuration among the three acceptors and thus the highest crystallinity. Different from the other two acceptors with minima at 0° and 180° , **SIDIC** shows a valley at 160-200°, suggesting that various twisted configurations with dihedral angles of 160-200° may exist, which leads to weak molecular packing and low crystallinity. Although TIDIC shows the lowest rotation energy barrier, the two stable configurations at 0° and 180° are all planar, thus TIDIC is more crystalline than SIDIC but less than DIDIC. These results indicate that acetylene linkage is an effective strategy to optimize the molecular packing and crystallinity of the acceptors.

A third morphological investigation technique was used to obtain further information about the donor and acceptor domain sizes in the BHJ blend. Fig. 6 presents the 2D smallangle X-ray scattering (GISAXS) patterns and the in-plane intensity profiles fitted with models reported elsewhere. 50 The pure FTAZ domain sizes of all the three films are fitted to be ~9 nm, mainly contributing to an intensity shoulder around 0.07 Å^{-1} , while the pure acceptor domain sizes of **FTAZ/SIDIC**, FTAZ/DIDIC and FTAZ/TIDIC films are estimated to be 11.4, 15.0 and 11.0 nm, respectively. Although each blend has similar domain sizes, the FTAZ/DIDIC film shows much stronger scattering intensity in the median q range, a signal of strong phase separation. The stronger crystallinity was also found in the GIWAXS data from the previous section as well. This might cause unsatisfactory miscibility and inefficient charge dissociation, leading to the worst IQE and $J_{\rm SC}$.

Conclusions

In summary, three novel FREAs (SIDIC, DIDIC and TIDIC) were designed and synthesized based on single bond, vinylene and acetylene linked IDT dimers and effects of the linking units on light absorption, energy levels, film morphology, charge transport, and photovoltaic properties were examined. Relative to SIDIC with single bond link, DIDIC with vinylene unit link

shows red-shifted absorption, while TIDIC with acetylene unit link shows blue-shifted absorption. Three molecules have similar LUMO levels, while TIDIC has a relatively lower HOMO level caused by electron-withdrawing acetylene bridge. TIDIC has a higher electron mobility than SIDIC and DIDIC. When blended with the donor FTAZ that has fitted energy levels and complementary absorption spectra, the TIDIC-based devices display higher $V_{\rm OC}, J_{\rm SC}$, FF and PCE than the SIDIC- and DIDIC-based OSCs.

Conflicts of interest

The authors declare no competing financial interest.

Acknowledgements

X. Z. wish to thank NSFC (21734001 and 51761165023). X. L. acknowledges the financial support from NSFC/RGC Joint Research Scheme (Grant No. N_CUHK418/17). J. J. R. and W. Y. thank the NSF (CBET-1639429) for financial support. J. L. thanks Natural Science Foundation of Guangdong Province (Grant No. 2019A1515011125) and Science and Technology Project of Shenzhen City (Grant No. JCYJ20190808173813204). The Supercomputing Center of Chinese Academy of Sciences is acknowledged for molecular modeling.

Notes and references

- 1 G. Yu, J. Gao, J. C. Hummelen, F. Wudl and A. J. Heeger, *Science*, 1995, **270**, 1789–1791.
- 2 G. Li, R. Zhu and Y. Yang, *Nat. Photonics*, 2012, **6**, 153–161.
- 3 L. Lu, T. Zheng, Q. Wu, A. M. Schneider, D. Zhao and L. Yu, *Chem. Rev.*, 2015, **115**, 12666–12731.
- 4 Y. Lin, Y. Li and X. Zhan, *Chem. Soc. Rev.*, 2012, 41, 4245–4272.
- 5 C. Yan, S. Barlow, Z. Wang, H. Yan, A. K. Y. Jen, S. R. Marder and X. Zhan, *Nat. Rev. Mater.*, 2018, 3, 18003.
- 6 P. Cheng, G. Li, X. Zhan and Y. Yang, *Nat. Photonics*, 2018, 12, 131–142.
- 7 J. Hou, O. Inganas, R. H. Friend and F. Gao, *Nat. Mater.*, 2018, 17, 119–128.
- 8 Y. Lin, J. Wang, Z. G. Zhang, H. Bai, Y. Li, D. Zhu and X. Zhan, *Adv. Mater.*, 2015, 27, 1170–1174.
- 9 Y. Lin, Q. He, F. Zhao, L. Huo, J. Mai, X. Lu, C. J. Su, T. Li, J. Wang, J. Zhu, Y. Sun, C. Wang and X. Zhan, *J. Am. Chem. Soc.*, 2016, 138, 2973–2976.
- 10 S. Chandrabose, K. Chen, A. J. Barker, J. J. Sutton, S. K. K. Prasad, J. Zhu, J. Zhou, K. C. Gordon, Z. Xie, X. Zhan and J. M. Hodgkiss, *J. Am. Chem. Soc.*, 2019, **141**, 6922–6929.
- 11 W. Liu, J. Zhang, Z. Zhou, D. Zhang, Y. Zhang, S. Xu and X. Zhu, *Adv. Mater.*, 2018, **30**, 1800403.
- 12 Z. Yao, X. Liao, K. Gao, F. Lin, X. Xu, X. Shi, L. Zuo, F. Liu, Y. Chen and A. K. Jen, *J. Am. Chem. Soc.*, 2018, **140**, 2054–2057.

- 13 J. Sun, X. Ma, Z. Zhang, J. Yu, J. Zhou, X. Yin, L. Yang, R. Geng, R. Zhu, F. Zhang and W. Tang, Adv. Mater., 2018, 30, 1707150.
- 14 J. Yuan, T. Huang, P. Cheng, Y. Zou, H. Zhang, J. L. Yang, S. Y. Chang, Z. Zhang, W. Huang, R. Wang, D. Meng, F. Gao and Y. Yang, Nat. Commun., 2019, 10, 570.
- 15 B. Kan, H. Feng, X. Wan, F. Liu, X. Ke, Y. Wang, Y. Wang, H. Zhang, C. Li, J. Hou and Y. Chen, J. Am. Chem. Soc., 2017, 139, 4929-4934.
- 16 Z. Xiao, S. Yang, Z. Yang, J. Yang, H. L. Yip, F. Zhang, F. He, T. Wang, J. Wang, Y. Yuan, H. Yang, M. Wang and L. Ding, Adv. Mater., 2019, 31, 1804790.
- 17 B. Jia, J. Wang, Y. Wu, M. Zhang, Y. Jiang, Z. Tang, T. P. Russell and X. Zhan, J. Am. Chem. Soc., 2019, 141,
- 18 Z. Fei, F. D. Eisner, X. Jiao, M. Azzouzi, J. A. Rohr, Y. Han, M. Shahid, A. S. R. Chesman, C. D. Easton, C. R. McNeill, T. D. Anthopoulos, J. Nelson and M. Heeney, Adv. Mater., 2018, 30, 1705209.
- 19 Y. Yang, Z. G. Zhang, H. Bin, S. Chen, L. Gao, L. Xue, C. Yang and Y. Li, J. Am. Chem. Soc., 2016, 138, 15011-15018.
- 20 M. Zhang, W. Gao, F. J. Zhang, Y. Mi, W. B. Wang, Q. S. An, J. Wang, X. L. Ma, J. L. Miao, Z. H. Hu, X. F. Liu, J. Zhang and C. L. Yang, Energy Environ. Sci., 2018, 11, 841-849.
- 21 S. Li, L. Ye, W. Zhao, S. Zhang, S. Mukherjee, H. Ade and J. Hou, Adv. Mater., 2016, 28, 9423-9429.
- 22 T. Liu, Z. H. Luo, Q. P. Fan, G. Y. Zhang, L. Zhang, W. Gao, X. Guo, W. Ma, M. J. Zhang, C. L. Yang, Y. F. Li and H. Yan, Energy Environ. Sci., 2018, 11, 3275-3282.
- 23 T. J. Aldrich, M. Matta, W. Zhu, S. M. Swick, C. L. Stern, G. C. Schatz, A. Facchetti, F. S. Melkonyan and T. J. Marks, J. Am. Chem. Soc., 2019, 141, 3274-3287.
- 24 S. Dai, F. Zhao, Q. Zhang, T. K. Lau, T. Li, K. Liu, Q. Ling, C. Wang, X. Lu, W. You and X. Zhan, J. Am. Chem. Soc., 2017, 139, 1336-1343.
- 25 Z. Luo, H. Bin, T. Liu, Z. G. Zhang, Y. Yang, C. Zhong, B. Qiu, G. Li, W. Gao, D. Xie, K. Wu, Y. Sun, F. Liu, Y. Li and C. Yang, Adv. Mater., 2018, 30, 1706124.
- 26 Y. Cui, H. Yao, J. Zhang, T. Zhang, Y. Wang, L. Hong, K. Xian, B. Xu, S. Zhang, J. Peng, Z. Wei, F. Gao and J. Hou, Nat. Commun., 2019, 10, 2515.
- 27 X. Xu, K. Feng, Z. Bi, W. Ma, G. Zhang and Q. Peng, Adv. Mater., 2019, 31, 1901872.
- 28 B. Fan, D. Zhang, M. Li, W. Zhong, Z. Zeng, L. Ying, F. Huang and Y. Cao, Sci. China: Chem., 2019, 62, 746-752.
- 29 J. Yuan, Y. Zhang, L. Zhou, G. Zhang, H.-L. Yip, T.-K. Lau, X. Lu, C. Zhu, H. Peng, P. A. Johnson, M. Leclerc, Y. Cao, J. Ulanski, Y. Li and Y. Zou, Joule, 2019, 3, 1140-1151.
- 30 Z. Zhou, W. Liu, G. Zhou, M. Zhang, D. Qian, J. Zhang, S. Chen, S. Xu, C. Yang, F. Gao, H. Zhu, F. Liu and X. Zhu, Adv. Mater., 2020, 32, 1906324.

- 31 L. Meng, Y. Zhang, X. Wan, C. Li, X. Zhang, Y. Wang, X. Ke, Z. Xiao, L. Ding, R. Xia, H. L. Yip, Y. Cao and Y. Chen, Science, 2018, 361, 1094-1098.
- 32 B. B. Fan, X. Y. Du, F. Liu, W. K. Zhong, L. Ying, R. H. Xie, X. F. Tang, K. An, J. M. Xin, N. Li, W. Ma, C. J. Brabec, F. Huang and Y. Cao, Nat. Energy, 2018, 3, 1051-1058.
- 33 J. Wang, J. Zhang, Y. Xiao, T. Xiao, R. Zhu, C. Yan, Y. Fu, G. Lu, X. Lu, S. R. Marder and X. Zhan, J. Am. Chem. Soc., 2018, 140, 9140-9147.
- 34 W. Gao, M. Zhang, T. Liu, R. Ming, Q. An, K. Wu, D. Xie, Z. Luo, C. Zhong, F. Liu, F. Zhang, H. Yan and C. Yang, Adv. Mater., 2018, 30, 1800052.
- 35 Y. Lin, T. Li, F. Zhao, L. Han, Z. Wang, Y. Wu, Q. He, J. Wang, L. Huo, Y. Sun, C. Wang, W. Ma and X. Zhan, Adv. Energy Mater., 2016, 6, 1600854.
- 36 Y. Q. Q. Yi, H. R. Feng, N. Zheng, X. Ke, B. Kan, M. J. Chang, Z. O. Xie, X. J. Wan, C. Li and Y. Chen, Chem. Mater., 2019, 31, 904-911.
- 37 Z. P. Yu, Z. X. Liu, F. X. Chen, R. Qin, T. K. Lau, J. L. Yin, X. Kong, X. Lu, M. Shi, C. Z. Li and H. Chen, Nat. Commun., 2019, 10, 2152.
- 38 S. Li, L. Zhan, F. Liu, J. Ren, M. Shi, C. Z. Li, T. P. Russell and H. Chen, Adv. Mater., 2018, 30, 1705208.
- 39 A. Meares, G. V. Bhagavathy, S. R. Zik, T. Gallagher and M. Ptaszek, J. Org. Chem., 2018, 83, 9076-9087.
- 40 G. Zhao, J. Liu, Q. Meng, D. Ji, X. Zhang, Y. Zou, Y. Zhen, H. Dong and W. Hu, Adv. Electron. Mater., 2015, 1, 1500071.
- 41 Y. Gao, J. Bai, Y. Sui, Y. Han, Y. Deng, H. Tian, Y. Geng and F. Wang, Macromolecules, 2018, 51, 8752-8760.
- 42 E. M. Espinoza, J. A. Clark, J. Soliman, J. B. Derr, M. Morales and V. I. Vullev, J. Electrochem. Soc., 2019, 166, H3175-H3187.
- 43 L. Dou, J. You, Z. Hong, Z. Xu, G. Li, R. A. Street and Y. Yang, Adv. Mater., 2013, 25, 6642-6671.
- 44 S. C. Price, A. C. Stuart, L. Yang, H. Zhou and W. You, J. Am. Chem. Soc., 2011, 133, 4625-4631.
- 45 W. Li, S. Albrecht, L. Yang, S. Roland, J. R. Tumbleston, T. McAfee, L. Yan, M. A. Kelly, H. Ade, D. Neher and W. You, J. Am. Chem. Soc., 2014, 136, 15566-15576.
- 46 V. Mihailetchi, L. Koster, J. Hummelen and P. Blom, Phys. Rev. Lett., 2004, 93, 216601.
- 47 I. Riedel, J. Parisi, V. Dyakonov, L. Lutsen, D. Vanderzande and J. C. Hummelen, Adv. Funct. Mater., 2004, 14, 38-44.
- 48 G. G. Malliaras, J. R. Salem, P. J. Brock and C. Scott, Phys. Rev. B: Condens. Matter Mater. Phys., 1998, 58, 13411-13414.
- 49 J. Mai, Y. Xiao, G. Zhou, J. Wang, J. Zhu, N. Zhao, X. Zhan and X. Lu, Adv. Mater., 2018, 30, 1802888.
- 50 J. Mai, T.-K. Lau, J. Li, S.-H. Peng, C.-S. Hsu, U. S. Jeng, J. Zeng, N. Zhao, X. Xiao and X. Lu, Chem. Mater., 2016, 28, 6186-6195.